NUMERICAL STUDIES OF HIGH CURRENT BEAM COMPRESSION IN HEAVY ION FUSION*

J. Bisognano and E. P. Lee
Lawrence Berkeley Laboratory
Berkeley, California 94702

James W-K. Mark
Lawrence Livermore National Laboratory
P.O. Box 808
Livermore, California 94550

The process of longitudinal compression of a drifting heavy ion pulse to be used as an ICF driver is examined with the aid of particle simulation. Space charge forces play a vital role in halting compression before the final focus lens system is reached. This must take place with minimal growth of transverse emittance and momentum spread. Of particular concern are the distortion of longitudinal phase space by the rounded transverse profile of the longitudinal self-electric field.

For application as an ICF reactor driver, a heavy-ion beam pulse must be longitudinally compressed by 1 to 2 orders of magnitude to achieve the peak power required to ignite a target.[1] This process, among others, will be tested in a facility known as the "High-Temperature Experiment"[2-6] in heavy-ion fusion. Beam compression is a critical element of an accelerator for heavy-ion fusion; it occurs primarily after the main phase of acceleration and before final focus onto target.

Here we examine the compression of a drifting heavy-ion pulse with the aid of particle simulations. We describe initial theoretical results for an in-principle solution to this problem. Further refinements including integration into a complete driver system are necessary before the least costly solution can be chosen.

An accelerated beam pulse has finite extent in space and time. Beam compression is initiated by firing the accelerating modules so that the tail end of the beam moves faster than the head. The variation of velocity is a linear function of distance (measured from the center of the pulse), this differential velocity can be viewed as a velocity "tilt" in longitudinal (z, v_z) phase space [see Fig. 1(a)]. At the end of beam compression, the tilt is removed and the compression is halted (and even reversed) by the longitudinal space-charge repulsion in the compressed beam bunch. (In the absence of finite space charge effects, the free-streaming velocity differentials and longitudinal emittance would instead be the determining factor for minimum beam length). Of course, we would have to impose external fields on the compressed beam to keep it compressed for any length of time. In practice, the beam bunch will be sent through the final focus lens system and onto the target before such expansion occurs. This entire process must be carefully controlled to produce the desired small spot on the fusion pellet. During compression, the transverse dimensions of the pulse must be controlled by alternating-gradient focusing.

*This work was supported by the Department of Energy Office of Energy Research under Contract No. DE-AC03-76SF00098 to Lawrence Berkeley Laboratory, and also Office of Inertial Fusion under Contract No. W-7405-ENG-48 to Lawrence Livermore National Laboratory.

Apart from the decrease in pulse length, it is also necessary to observe the requirements on the final beam pulse necessary to focus it onto a target at a particular focal distance. Of particular importance in the present context are second order chromatic aberrations which for rough illustrative purposes provide a condition

$$r_{spot} > 2\left(\frac{\Delta p_z}{p_z}\right)_{lens}\left(r_{max}\right)_{lens} \quad . \tag{1}$$

Here $r_{spot} \approx 0.1$ cm is the envelope radius of the desired focal spot, $(r_{max})_{lens} \approx 10$ cm is the envelope radius at the final focus lens, and $\Delta p_z/p_z$ is the full width in the dispersion of z momenta (accumulated from all sources) at final focus. These typical numbers imply that $\Delta p_z/p_z < 0.01$.

A second condition is that the transverse emittance ϵ must be sufficiently small. To limit the effect of spherical aberrations in the final lens, the half-angle of the focal cone must satisfy

$$\theta_s < 0.02 \text{ rad.} \tag{2}$$

Using the emittance determined spot radius $r \gtrsim \epsilon/\theta$, this translates into the condition $\epsilon \lesssim 2 \times 10^{-3}$ cm$\cdot$rad, which applies after final compression.

A simplified analytic solution obtains if we adopt the model of a one-dimensional beam that has no longitudinal momentum spread Δp_z at any z before beam compression. The space-charge self field of the beam bunch is approximated by the electric field

$$E_z = -g\frac{\partial\lambda}{\partial z} \quad , \tag{3}$$

where $\lambda(z, t)$ is line charge density; and g is a coupling applicable to long-wavelength disturbances. In this regime g has the value

$$g \approx \frac{1}{4\pi\epsilon_0}\left(\log\frac{b^2}{a^2} + \frac{1}{2}\right) . \tag{4}$$

In this idealized limit, the beam pulse obeys one-dimensional fluid equations in λ and v_z, where $v_z(z, t)$ is beam internal velocity. We can obtain an exact solution with a parabolic longitudinal profile for λ

$$\lambda(z, t) = \frac{\lambda_0 L_0}{L(t)}\left[1 - 4\,\frac{(z-\bar{z})^2}{L^2(t)}\right], \tag{5a}$$

$$v_z(z, t) = \bar{v} + (z - \bar{z})\frac{d}{dt}\ln L(t) \quad , \tag{5b}$$

This simplified solution provides a useful guide to an in-principle solution of the beam compression process provided that it survives under the realistic, multidimensional environment of actual pulses. In the present case the constant factor g is replaced by a radius-dependent term characteristic of actual beams, so that particles at different radii r are acted on by different longitudinal self-forces and experience different evolution, resulting in growth of Δp_z at each point in the pulse.

An estimate that g varies over r by ±20% results in the evolution of phase space (z, v_z) and line density $\lambda(z, t)$ shown in Figs. 1 and 2. These results were obtained using our one-dimensional particle-simulation code BLISS, which uses the field of Eq. (3). Although actual transverse particle motions average over actual spread of g with radius, this one-dimensional model assigns each particle a g-factor appropriate only to its initial position.

As expected, the initial momentum tilt $(\Delta p_z/p_z) \approx 4\%$ of Fig. 1(a) is stopped in Fig. 1(c), but at the expense of some momentum spread $\Delta p_z/p_z$. The simulated problem corresponds to the situation typical of the High-Temperature Experiment, in which a 1.875-μC, 125-MeV beam of singly ionized sodium will be compressed from a length of 10 m to a final length (according to our analytic model) of 1 m. Since the model shows that space-charge effects are important only in the last 2 m of compression, our simulation concentrates on this phase.

We also used a two-dimensional LLNL version of the particle code MASK[7] to repeat the one-dimensional simulation, with realistic variation of g with r automatically included in the force calculations. The initial momentum spread $\Delta p_z/p_z \approx 4\%$ results in a final momentum spread $\Delta p_z/p_z < 0.5\%$ in this simulation (Figs. 3 and 4). This final $\Delta p_z/p_z$ is comparable to that found for the one-dimensional simulation, with its artificially spread g-factor.

The two-dimensional simulation again uses a 1.875-μC, 125-MeV beam of Na^+ ions. The beam radius has the value a = 1 cm, and the perfectly conducting pipe has radius b = 2 cm. The boundary conditions at $z \to \pm\infty$ are approximated accurately by doubling the periodicity length of the simulation region in z, because the Green's function falls off exponentially. The transverse quadrupole focusing forces are approximated by the axially symmetric radial electric field

$$E_r = -5.266 \times 10^6 \frac{r}{b} \text{ V/m} \quad . \tag{7}$$

A total of 46,751 particles are used on a 20 x 512 grid, representing a region 2 cm x 2 m in the r and z directions, respectively. The initial line density $\lambda(z, 0)$ is made nearly parabolic by the superposition of 20 constant-charge-density and constant-radius (r = a) components. Each such component is loaded with a Maxwellian velocity distribution with

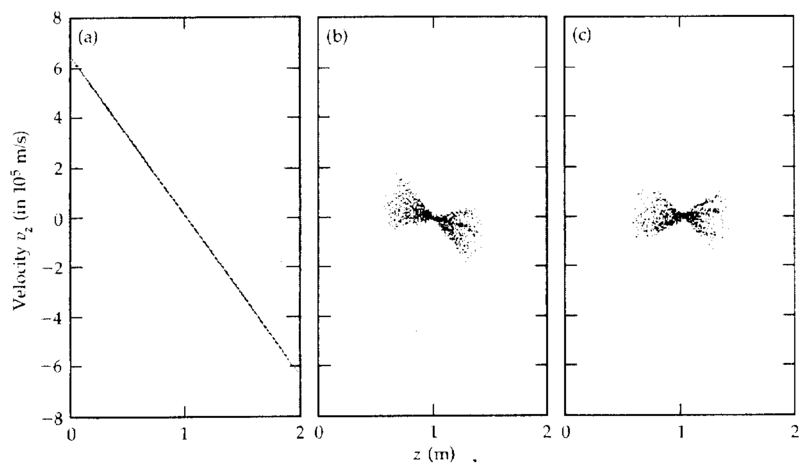

Fig. 1. The (z, v_z) phase space of the 1-D particle-code simulation (see text) at (a) t = 0 (initial velocity tilt), (b) t = 0.7 μs, (c) t = 1.5 μs (final compressed state).

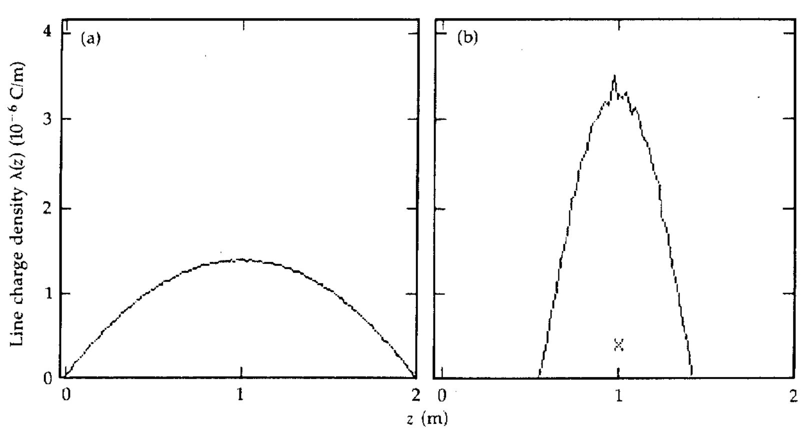

Fig. 2. Spatial line densities $\lambda(z, t)$ of particles in the 1-D simulation of Fig. 1 at (a) t = 0, (b) t = 1.5 μs.

$$\overline{v_{\perp}^2}_i = \frac{2i - 1}{20}\theta \quad , \quad i = 1, \ldots, 20 \quad , \qquad (8)$$

where θ characterized the required $\overline{v_{\perp}^2}$ at $z = 0$ for the parabolic distribution. Note that $\overline{(2i - 1)/20} = 1$, so that loading according to Eq. (8) gives the correct $\overline{v_{\perp}^2}$.

In Figs. 3 and 4, 10% of the particles are plotted. As the beam is compressed, an efficient use of the simulation grid is made by allowing the beam to expand in r at fixed effective focusing forces while the space-charge self-fields increase to a dominant level, so that the beam radius almost reaches the pipe radius.

In Summary, transverse beam spread need not be an impediment to the longitudinal beam compression needed in heavy-ion fusion to increase peak power by 1 to 2 orders of magnitude. Additional work is necessary to develop a complete understanding for a range of initial conditions. In particular, the parabolic beam line density $\lambda(z, 0)$ introduced above (because of the existence of an analytical model for this profile) uses focusing forces inefficiently; a nearly flat $\lambda(z, 0)$ is preferable in the regard. Also needed are additional studies of multidimensional effects introduced by beam misalignments and by the accumulation of realistic jitters in acceleration forces. Effects of initial beam temperature in the longitudinal direction must also be introduced.

References

[1] A. Faltens, E. Hoyer, and D. Keefe, "A 3 Megajoule Heavy-Ion Fusion Driver," in High Power Beams 81, H. J. Doucet and J. M. Buzzi, Eds., Ecole Polytechnique, Palaiseau, France, 1981, pp. 751-758.

[2] R. O. Bangerter, "The U.S. Program in Heavy-Ion Fusion," Los Alamos National Laboratory, Los Alamos, N. Mex., LA-UR-82:1192 (1982).

[3] "A Proposed Program to Develop Linear Induction Accelerator Technology in Support of the National Accelerator Inertial Fusion Plan," Lawrence Berkeley Laboratory, Berkeley, Calif., LBL PUB-5065, 1982.

[4] J. W-K. Mark et al., "Heavy-Ion Inertial Fusion: Suggested Experiments on Disk Heating and Beam Transport Using Accelerator Test Facilities," in High-Power Beams 81, H. J. Doucet and J. M. Buzzi, Eds., Ecole Polytechnique, Palaiseau, France, 1981, pp. 649-656.

[5] J. W-K. Mark, "Recent U.S. Target Physics Related Research in Heavy Ion Fusion," in Proc. Symp. on Accelerator Aspects of Heavy Ion Fusion, D. Boehne, Ed., Gesellschaft für Schwerionenforschung, Darmstadt, W. Germany, GSI-82-8, 1982.

[6] E. P. Lee and J. W-K. Mark, "Studies for the High Temperature Experiment in Heavy-Ion Fusion," Laser Program Annual Report 83, Lawrence Livermore National Laboratory, Livermore, Calif., UCRL-50021-83, 1984, pp. 3-13 to 3-21.

[7] A. Palevsky, "Generation of Intense Microwave Radiation by the Relativistic e-Beam Magnetron (Experiment and Numerical Simulation)", Ph.D. thesis, Massachusetts Institute of Technology, Cambridge, Mass., 1980.

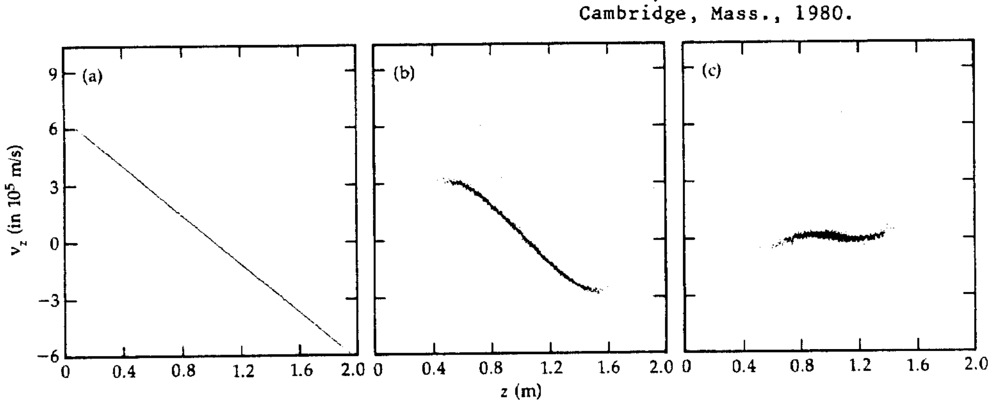

Fig. 3. The (z, v_z) phase space of the 2-D particle-code simulation (see text) at (a) $t = 0$ (initial velocity tilt), (b) $t = 0.7$ μs, (c) $t = 1.4$ μs (final compressed state).

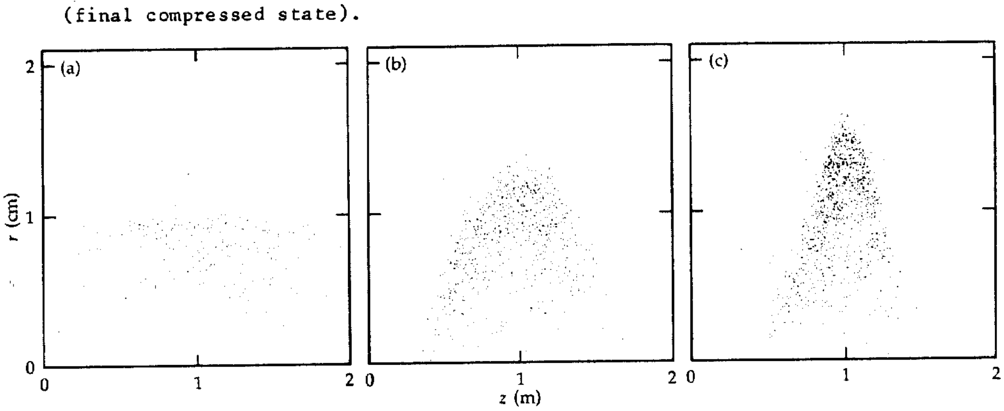

Fig. 4. The spatial positions in (r, z) coordinates of 10% of the particles in the 2-D simulation of Fig. 3, at corresponding times. Note the different horizontal and vertical length scales.